Applied Catalysis B: Environmental 256 (2019) 117807

Contents lists available at ScienceDirect

Applied Catalysis B: Environmental

journal homepage: www.elsevier.com/locate/apcatb

Active and stable Pt-Ceria nanowires@silica shell catalyst: Design, formation mechanism and total oxidation of CO and toluene

Honggen Peng[a,b], Tao Dong[a], Li Zhang[a], Caili Wang[a], Wenming Liu[a], Jiafeng Bao[c], Xiang Wang[a], Ning Zhang[a], Zheng Wang[d], Peng Wu[e], Pengfei Zhang[c,*], Sheng Dai[b,f,**]

[a] Key Laboratory of Jiangxi Province for Environment and Energy Catalysis, College of Chemistry, Nanchang University, Nanchang, 330031, PR China
[b] Chemical Sciences Division, Oak Ridge National Laboratory, Oak Ridge, TN, 37830, United States
[c] School of Chemistry and Chemical Engineering, Shanghai Jiao Tong University, Shanghai, 200240, PR China
[d] State Key Laboratory of High-efficiency Utilization of Coal & Green Chemical Engineering, Ningxia University, Yinchuan, 750021, PR China
[e] Shanghai Key Laboratory of Green Chemistry and Chemical Processes, Department of Chemistry and Molecular Engineering, East China Normal University, North Zhongshan Road 3663, 200062, Shanghai, PR China
[f] Department of Chemistry, University of Tennessee, Knoxville, TN, 37996 United States

ARTICLE INFO

Keywords:
Ceria nanowires
Mesoporous materials
Self-assembly
Core-shell catalysts
VOCs combustion

ABSTRACT

Cerium oxide is one of the most important rare earth metal oxides in catalysis, however, the sintering problem of noble metals and CeO_2 at higher temperature (*e.g.*, > 700 °C) is still unresolved. Herein, Pt nanoparticles self-assembled on ultra-thin CeO_2 nanowires (NWs) and then confined inside a thermally robust porous silica shell (Pt-CeO_2NW@SiO_2) were introduced. The thickness of CeO_2 NWs was just ~2.0 nm. Moreover, Pt-CeO_2 NW@SiO_2 showed significantly enhanced catalytic performances for total oxidation of CO and toluene. The increased catalytic properties are attributed to the strong metal-support interaction effect between Pt and CeO_2 NWs at sub-nanoscale. Most importantly, the special core-shell structure also affords excellent sintering resistance retention up to 700 °C for 100 h, due to the guarding effect of porous silica shell. Finally, the formation mechanism of Pt-CeO_2 NW@SiO_2 was investigated in detail. Current strategy should inspire many rational designs of rare-earth metal-based nanocatalysts for real-world catalysts.

1. Introduction

Total oxidation of carbon monoxide (CO) [1–3] and volatile organic compounds (VOCs) [4–9] is an important topic in environmental catalysis, while Pt/CeO_2 is one promising catalyst toward this target. [10–18] From the proof of principle, CeO_2 with high oxygen storage capacity and abundant oxygen vacancy defects between Ce^{3+} and Ce^{4+} oxidation states can benefit the charge transfer and oxygen migration, [19–21] meanwhile, Pt species function well for C—C and C—H bond activation, especially at moderate and high temperatures [22]. Generally, a strong interaction exists between CeO_2 and Pt species, which results in highly active sites locating at the interface between CeO_2 and Pt species, [23–26] the so called interfacial catalysis [27–32]. Actually, Pt/CeO_2 hybrids with many well-defined morphologies, such as nanorod, nanocube, have been studied intensively. [33–37] To maximum the active interface, Pt/CeO_2 nanowire with uniform dispersion of Pt and ceria species are of great interest.

Actually, metal nanowires have already shown attractive performance in many processes. [38–40] Whereas their thermal stability is far from ideal, because the nanowires themselves with high surface energy tend to sinter, distort and aggregate into larger nanoparticles under high temperature reaction, leading to loss of the original superior properties. Therefore, developing a strategy to prevent the sintering of the metal nanowires remains a challenging issue for the commercialization of metal nanowire-based catalysts [41]. Although a silica coating strategy has been used in palladium-ceria nanowire system [42], the formation mechanism—an important study to bring up a new principle—was missed.

Herein, we show an in-situ self-assembly method to prepare, the Pt-CeO_2 nanowire@SiO_2 catalyst, with a core-shell structure that comprises of a self-assembled Pt-CeO_2 nanowire (NW) as the core and microporous silica as the shell. The thickness of ceria nanowires was just 2.0 nm, which could be considered as the thinnest ceria nanowires, to the best of our knowledge. More importantly, the formation mechanism

* Corresponding author.
** Corresponding author at: School of Chemistry and Chemical Engineering, Shanghai Jiao Tong University, Shanghai, 200240, PR China
E-mail addresses: chemistryzpf@sjtu.edu.cn (P. Zhang), dais@ornl.gov (S. Dai).

https://doi.org/10.1016/j.apcatb.2019.117807
Received 24 March 2019; Received in revised form 26 May 2019; Accepted 30 May 2019
Available online 04 June 2019
0926-3373/

of this novel material was also investigated in detail. Finally, we investigate the catalytic performance of the core-shell catalyst containing rare earth nanowires self-assembled with Pt NPs, and interestingly Pt-CeO_2 NW@SiO_2 catalyst shows excellent catalytic performance for CO and toluene total combustion. The CO and toluene oxidation reach 100% conversion at 70 °C and 170 °C, respectively, which is far better than the performance of control catalysts by impregnation method. The Pt-CeO_2 NW@SiO_2 also has superior thermal stability due to enclosing the Pt-CeO_2 nanowires in porous silica shell.

2. Experimental

2.1. Catalyst preparation

2.1.1. Synthesis of Pt-CeO_2NW@SiO_2, Pt@SiO_2 and CeO_2NW@SiO_2

Pt-CeO_2 NW@SiO_2 was synthesized in a reverse-micelle emulsion system according to our previous reported literature with some modifications. [42]. The method for synthesis of Pt@SiO_2 and CeO_2NW@SiO_2 was similar with Pt-CeO_2NW@SiO_2 just without adding the precursors of $Ce(NO_3)_3{\cdot}6H_2O$ and $Pt(NH_3)_4(NO_3)_2$, respectively. The above method and procedure was also used to synthesize the pure silica nanospheres by using deionized water in place of aqueous solution of Pt $(NH_3)_4(NO_3)_2$ and $Ce(NO_3)_3{\cdot}6H_2O$. During the synthesis of 2%Pt-CeO_2NW@ SiO_2 and CeO_2NW@SiO_2 catalyst, a few drops of liquid from the round bottom flask before adding TEOS were extracted to investigate its plausible formation mechanism. The detailed procedures could be found in Supporting Information.

2.1.2. Synthesis of Pt-CeO_2/SiO_2 and Pt/SiO_2

For comparison, traditional catalysts with Pt and Pt-CeO_2 supported on SiO_2 nano-spheres were also synthesized through conventional impregnation method (0.02 g $Pt(NH_3)_4(NO_3)_2$ and 0.02 g $Pt(NH_3)_4(NO_3)_2$ with 0.03 g $Ce(NO_3)_3{\cdot}6H_2O$ impregnated with 0.5 g SiO_2 spheres). After impregnation, the samples were dried in a vacuum oven at 80 °C for 12 h, and calcined in air at 500 °C for 4 h, then, reduced in 10%H_2/N_2 at 400 °C for 4 h to obtain the final 2%Pt/SiO_2 and 2%Pt-CeO_2/SiO_2 samples. The Pt contents for all the five samples are similar to the original values of the catalysts synthesis within the experimental error which determined by Inductively Coupled Plasma-Optical Emission Spectrometry (ICP-OES) method. The Ce contents for three catalysts are the same, which is ~2%(wt) and also confirmed by ICP-OES method.

2.1.3. Synthesis of 1%Pt-CeO_2 NW@SiO_2-HNO_3

To study the effect of CeO_2 on catalytic performance of Pt-CeO_2NW@SiO_2, 1%Pt-CeO_2 NW@SiO_2 sample was treated in a certain amount of concentrated nitric acid at 70 °C for 2 h to remove the CeO_2 nanowires. The resulting sample was calcined in air atmosphere at 500 °C for 4 h, then reduced in 10%H_2/N_2 at 400 °C for 4 h. The final catalyst is denoted as 1%Pt-CeO_2 NW@SiO_2 -HNO_3.

2.2. Catalyst characterization

X-ray diffraction (XRD) patterns, hydrogen temperature programmed reduction (H_2-TPR), carbon monoxide temperature programmed desorption (CO-TPD), transmission electron microscopy (TEM), scanning TEM (STEM), line scan and elemental mapping images, nitrogen adsorption-desorption analysis, X-ray photoelectron spectrum (XPS), inductively coupled plasma optical emission spectrometry (ICP-OES) and *in situ* diffuse reflectance infrared Fourier transform spectroscopy (DRIFT) measurements were performed to characterize the physical, chemical and reaction process of the catalysts. The detailed characterization methods were shown in Supporting Information.

2.3. Catalytic activity test

2.3.1. Carbon monoxide (CO) oxidation

All the catalysts were evaluated for CO oxidation as a model reaction in a continuous flow reactor with a gas composition of 1% CO, 21% O_2 and balanced by high purity N_2 [8,43]. Typically, 50 mg of catalyst was used for each measurement with a flow rate of 30 ml min^{-1}, which corresponds to a weight hourly space velocity (WHSV) of 36,000 ml h^{-1} g^{-1}. The reactants and products were analysized on-line on a GC9310 gas chromatograph equipped with a TDX-01 column and a TCD detector.

2.3.2. Toluene total oxidation

The catalysts were also evaluated for toluene total oxidation in a quartz tube (Inner Diameter = 6 mm) reactor with a continuous flow over 30 mg catalyst, which is similar to our previous report. [7] The detailed activity test process was presented in Supporting Information.

3. Results and discussion

3.1. Characterization of Pt-CeO_2NW@SiO_2

The transmission electron microscope (TEM) images in Fig. 1(a) and (b) displayed that the Pt-CeO_2 NW@SiO_2 with perfect wormlike core@shell structure was synthesized. It is clearly observed that elongated Pt-CeO_2 NWs are all embedded in silica shell. The dimension of these Pt-CeO_2 nanowires is just around 2.0 nm. HRTEM was adopted to confirm the crystal structure (Fig. 1(c)). The Pt-CeO_2 NW@SiO_2 sample shows the typical planes of 0.28 nm and 0.32 nm for the (200) and the (111) lattice planes of CeO_2, respectively. The lattice plane of 0.22 nm agrees well with (111) characteristic plane of Pt metal. The Fast Fourier Transform (FFT) pattern (inset of Fig. 1(c)) described three dim rings corresponding to (111) and (200) plane of the CeO_2 phase and the (111) plane of Pt metal, which further proves that the formation of self-assembled Pt-CeO_2 nanowires. Furthermore, high-angle annular dark-field STEM (HAADF-STEM) technique was used to determine the morphology structure. The Pt an Ce species are located in the center of the silica shell networks (see Fig. 1(d)). This result was further confirmed by the line scan technique, the self-assembled Pt-CeO_2 nanowires were loaded in the center of the Pt-CeO_2 NW@SiO_2 sample (Fig. 1(d) inset).

The HAADF-STEM mapping technique was also used for analysis of the distribution of the Pt, O, Si and Ce components in the nanostructures. As shown in the images presented in Fig. 2(a–e), the Si element spreads in the whole particle. The Ce element signal could not be found in the shell position but only appeared in the core position, and the Pt element existed in the similar position with Ce element, thus indicating that Pt nanoparticles deposit on the CeO_2.

Additionally, XPS measurements were performed to identify the surface compositions and chemical valence of Pt-CeO_2 NW@SiO_2 and the control sample (Pt-CeO_2/SiO_2 prepared via impregnation method). XPS result reveals that the Pt-CeO_2NW@SiO_2 and Pt-CeO_2/SiO_2 afford two energy peaks at 71.6 and 75.1 eV, which are typical bands for the Pt $4f_{7/2}$ and Pt $4f_{5/2}$ electrons of metallic Pt^0 (Fig. 1(e)). No peaks corresponding to Pt^{2+} were observed, which demonstrated that all the Pt^{2+} species had been reduced by H_2 [44]. Obviously, the intensity of two peaks for Pt $4f_{7/2}$ and Pt $4f_{5/2}$ electrons in Pt-CeO_2NW@SiO_2 catalyst is weaker than that of Pt-CeO_2/SiO_2, indicating that Pt is mainly coated by SiO_2 in core-shell structure. Over Ce 3d XPS spectra, two prominent bands at 884.4 and 904.0 eV in the Pt-CeO_2/SiO_2 catalyst can be ascribed to the Ce $3d_{5/2}$ and Ce $3d_{3/2}$, respectively (Fig. 1(f)).

It is hard to detect the peaks for Ce from the wide scan survey of Pt-CeO_2NW@SiO_2 nanocomposite, which also suggests that the majority of CeO_2 nanowires were really coated by a silica layer, forming a perfect core–shell structure. It is well known that XPS technique is usually applied to characterize the surface composition of materials and its detectable depth is no more than 10 nm. [42] Thus, if Pt-CeO_2

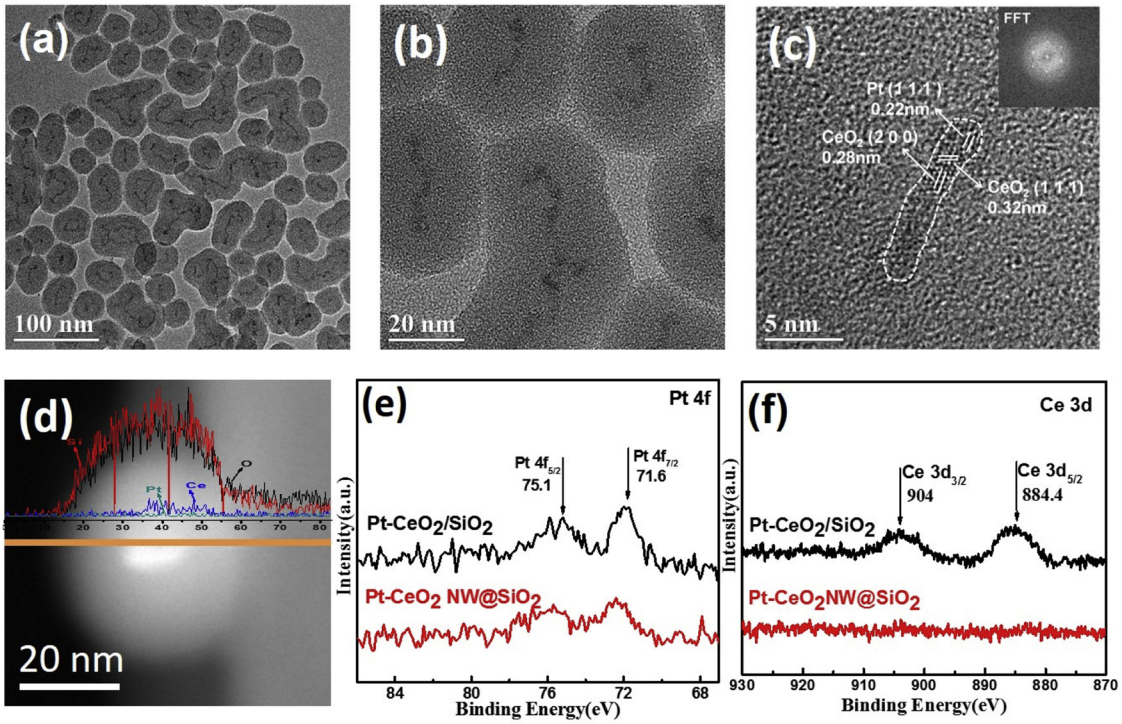

Fig. 1. TEM and HRTEM images (a, b, c) and HAADF-STEM image (inset is line scan) (d) of Pt-CeO_2 NW@SiO_2, XPS profiles of Pt4f and Ce3d for Pt-CeO_2 NW@SiO_2 and Pt-CeO_2/SiO_2 catalysts (e, f).

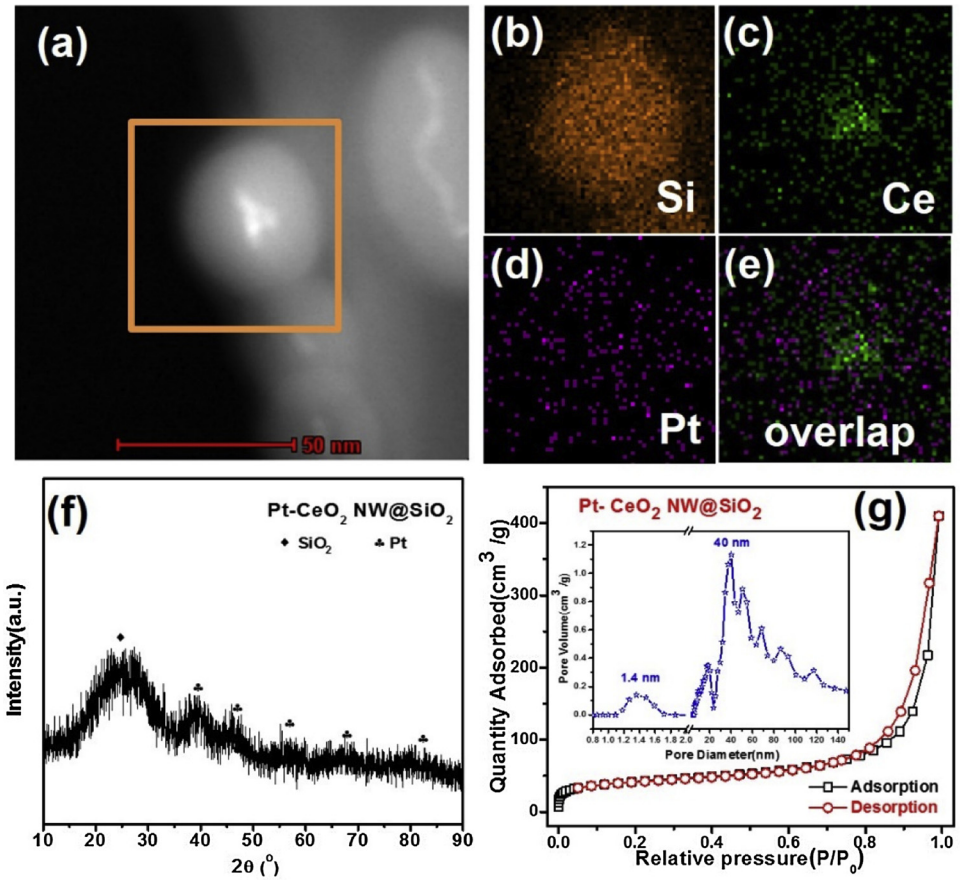

Fig. 2. HAADF-STEM EDX Mapping (a–e), XRD pattern (f) and N_2 adsorption/desorption isotherm and pore size distribution (inset) (g) of Pt-CeO_2 NW@SiO_2.

nanowires are embedded by the SiO_2 outer shell and it is thick enough, which is legitimate that no or weak bands of Pt and Ce signals could be detected. Therefore, all the TEM, line scanning and XPS results confirm that the Pt-CeO_2 NW@SiO_2 nanocomposite has been successfully synthesized.

To identify the crystal structure of those catalysts, the XRD analysis was performed. As displayed in Fig. 2(f) and Fig. S1, all the samples have one broad peak at 2θ of 15 to 35°, which is the typical pattern of amorphous silica. Another five weak diffraction bands at 2θ of 39.7°, 46.2°, 67.4°, 81.2°, 85.7° are observed, which are assigned to the (111), (200), (220), (311), and (222) facets of Pt^0 (PDF#04-0802). Apparently, the diffraction peaks of Pt in Pt-CeO_2NW@SiO_2 catalysts is weaker, which is a testimony of their high dispersity, and it will be further confirmed by CO chemsorption. There were no diffraction peaks relating to CeO_2, which is ascribed to the low content loading of CeO_2 and the shield effect of silica shell, thus escaping the detection of XRD. It is reasonable because the Pt- CeO_2 nanowire cores are embedded in SiO_2 shells.

The texture structures of the samples were then determined by N_2 sorption technique at 77 K, and the results are presented in Fig. 2(g), Fig. S2, and Table S1. All five catalysts show an increasing N_2 uptake in p/p_0 between 0.6 and 0.9, which is characteristic of mesoporous materials. The mesopores in Pt-CeO_2 NW@SiO_2 (6–40 nm) may be derived from the particle assembling, which is in line with the TEM results displayed in Fig. 1(b). The porous silica shell (˜1.4 nm) was obviously seen from the N_2 sorption analysis, which is an important channel to make gas reactants access to active Pt-CeO_2 core.

3.2. Plausible formation mechanism of Pt-CeO_2NW@SiO_2

In order to explore the formation mechanism of Pt-CeO_2 NW@SiO_2 with core-shell structure, a part of the liquid suspension before adding the silica source (TEOS) into the synthetic process was extracted to perform the TEM characterization. The TEM images (Fig. 3. Fig. 3(a and b)) clearly show the presence of typical nanowire structure yet without silica layers, which are considered to be Pt(OH)x-Ce(OH)x nanowires. The dark dots on the nanowires indicate the presence of Pt-based nanoparticles. Furthermore, HAADF-STEM technique was adopted to measure the distribution of Pt, Ce and O elements over the self-assembled Pt(OH)x-Ce(OH)x nanowires (Fig. 3(c–g)). The Pt, Ce and O elements are spread homogeneously over the nanowires. Thus, we here consider that the formation of Pt(OH)x-Ce(OH)x starts with the growth of Ce(OH)x nanowires.

In order to figure out this process, we carried out a control experiment to prepare $Ce(OH)_x$ nanowires, namely, keeping the same synthetic conditions yet without the addition of the Pt precursor. Interestingly, we did obtain the relevant products of $Ce(OH)_x$ nanowires (Fig. 4(a and b)). The uniform nanowires without the heavy dark dots indicate the presence of pure $Ce(OH)_x$ nanowires. Moreover, the CeO_2 nanowires can also be embedded in SiO_2 shell (Fig. 4(c and d)), which strongly supported our above-mentioned viewpoint. It should be regarded that the ceria nanowires were synthesized in inverse microemulsion system for the first time. As far as we know, this kind of ceria nanowire was the thinnest one among the reported literatures (Table S2), whose width is only ˜2.0 nm. We deduced that the formation mechanism of Pt-CeO_2 nanowires includes: a) Pt nanoparticles supported on $Ce(OH)_x$ nanowires to form $Pt(OH)_x$-$Ce(OH)_x$ nanowires *via* a self-

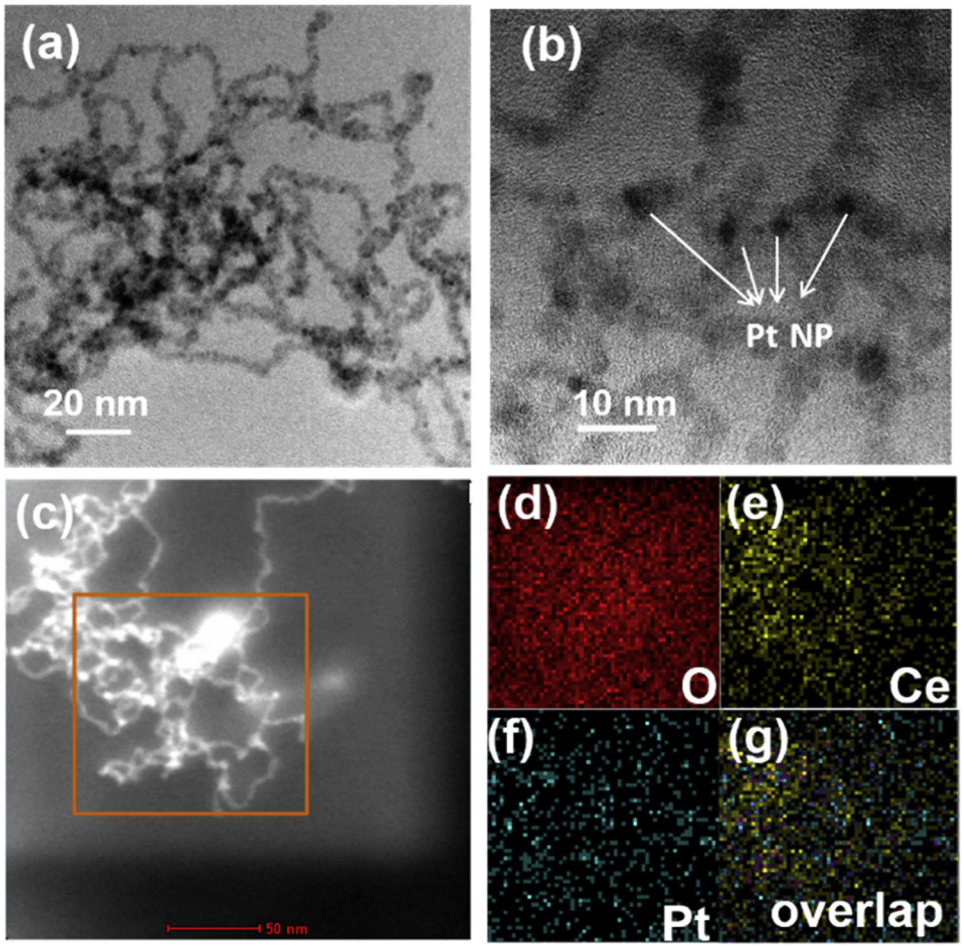

Fig. 3. TEM images (a and b) and HAADF-STEM EDX Mapping of Pt-Ce(OH)x NW(c –g).

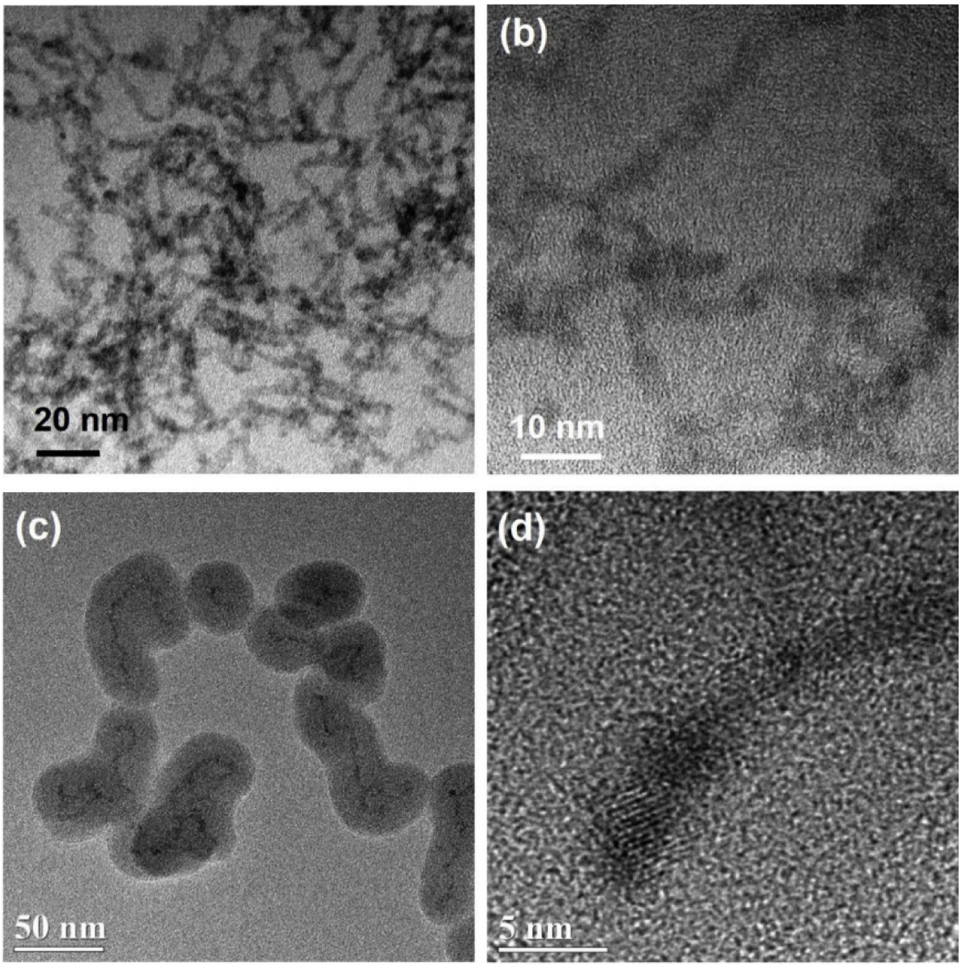

Fig. 4. TEM images of Ce(OH)x NW (a and b) and CeO_2 NW@SiO_2(c and d).

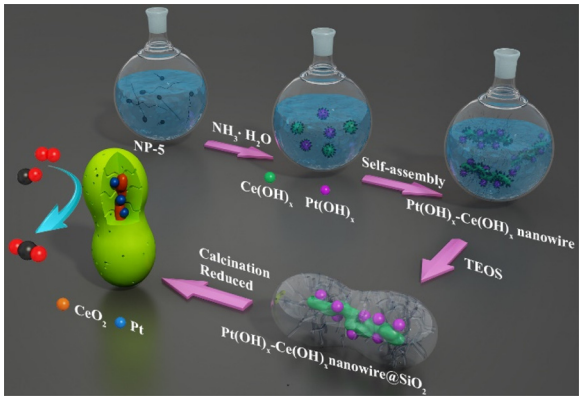

Scheme 1. A plausible formation mechanism of Pt-CeO_2 NW@SiO_2.

assembly process; b) The TEOS was hydrolyzed along the nanowires to form the elongated wormlike shell, leading to Pt-CeO_2 nanowires after calcining and reducing.

The plausible formation mechanism of Pt-CeO_2 NW@SiO_2 by the inverse microemulsion method was described in Scheme 1. Pt$(NH_3)_4(NO_3)_2$, $Ce(NO_3)_3{\cdot}6H_2O$, and tetraethylorthosilicate (TEOS) were chosen as the core and shell precursors, respectively. In the first step, Pt$(NH_3)_4(NO_3)_2$ and $Ce(NO_3)_3{\cdot}6H_2O$ aqueous solution was dropped into the water-in-oil (w/o) reverse micelle system. After adding the aqueous $NH_3{\cdot}H_2O$ to the above system, the nucleation, growth and self-assembly of $Pt(OH)_x$ NPs and $Ce(OH)_x$ NWs, result in $Pt(OH)_x$-$Ce(OH)_x$ nanowires in micelle system. When TEOS was added, the hydrolysis of TEOS by aqueous $NH_3{\cdot}H_2O$ would proceed on the interface between water and oil, leading to the encapsulation of $Pt(OH)_x$-$Ce(OH)_x$ nanowires in silica shell. Subsequently, the obtained $Pt(OH)_x$-$Ce(OH)_x$ NW@SiO_2 species were separated by centrifugation, washing and drying. Then, the sample was calcined and reduced in air and H_2 atmosphere. Therefore, the Pt-CeO_2 NW@SiO_2 catalyst were obtained via embedding the self-assembled Pt-CeO_2 nanowires inside silica shell.

3.3. Reducibility of Pt-CeO_2 NW@SiO_2 and related catalysts

Hydrogen temperature programed reduction (H_2-TPR) experiments were performed to study the reducibility of the 2%Pt-CeO_2 NW@SiO_2, 2%Pt-CeO_2/SiO_2 and 2%Pt@SiO_2 catalysts. The H_2-TPR profiles are presented in Fig. 5. For the 2%Pt@SiO_2 sample, there was no signal of reduction. Because the three catalysts were reduced in 10%H_2/N_2 at 400 °C for 4 h to completely reduce the Pt species. For the 2%Pt-CeO_2/SiO_2 sample, the reduction peak at ~415 °C was attributed to the reduction of surface Ce^{4+} to Ce^{3+} species, while the reduction peak centered at ~535 °C was owing to the reduction of the bulk Ce^{4+} species to Ce^{3+}. Over 2%Pt-CeO_2 NW@SiO_2, two main reduction peaks are found at 489 °C and 684 °C, respectively. However, in comparison to the 2%Pt-CeO_2/SiO_2 synthesized *via* impregnation method, the reduction peak of 2%Pt-CeO_2 NW@SiO_2 has moved toward high temperature after optimization of the catalyst structure, which indicates that the encapsulated Pt-CeO_2 NW has a more intimate contact with the microporous silica, compared with the 2%Pt-CeO_2/SiO_2 sample. This phenomenon was also observed by many other related core-shell

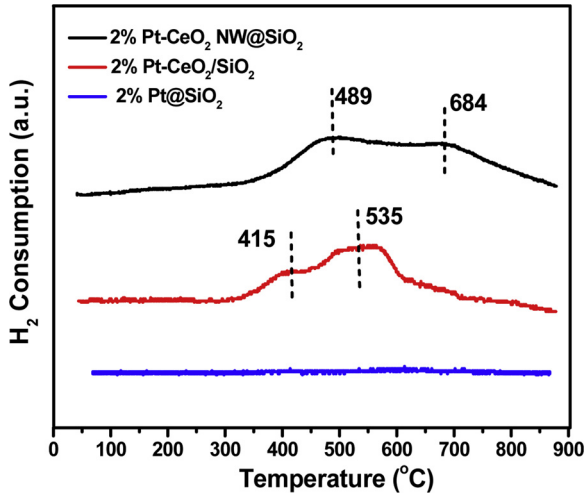

Fig. 5. H_2-TPR profiles of 2%Pt-CeO_2 NW@SiO_2 and related catalysts.

catalysts. [42,45–47] In addition, the formation of more Pt-CeO_2 interfaces may also increase their strong metal-support interaction and attribute to its higher reduction temperature.

3.4. Catalytic performances of Pt-CeO_2NW@SiO_2

The carbon monoxide (CO) oxidation reaction was chosen as one of the model reactions to test the catalytic performance of Pt-CeO_2NW@SiO_2 and related catalysts. The activity results were displayed in Fig. 6(a). The weight hourly space velocity (WHSV) of the CO oxidation reaction was fixed at 36 000 mL h^{-1} g^{-1}. It is convenient to compare the catalytic activity of these catalysts by using the reaction temperatures of T_{10}, T_{50}, and T_{90} (temperatures of CO conversion at 10%, 50% and 90%, respectively), as listed in Table S2. For all of the five samples, 2%Pt-CeO_2 NW@SiO_2 is the most active, followed by 1%Pt-CeO_2NW@SiO_2 and 2%Pt@SiO_2. For example, the temperature of T_{50} is 51 °C over 2%Pt-CeO_2 NW@SiO_2, 76 °C over 1%Pt-CeO_2 NW@SiO_2, and 103 °C over 2%Pt@SiO_2. For the 2%Pt/SiO_2 and 2%Pt-CeO_2/SiO_2 samples, both of them show low catalytic activity, which can be seen that their T_{50} reached up to 142℃ and 124℃, respectively. For converting CO to CO_2, the 100% conversion temperatures of these samples follow the sequence of 2%Pt /SiO_2 (150 °C) < 2%Pt-CeO_2/SiO_2 (130 °C) < 2% Pt@SiO_2 (110 °C) < 1%Pt-CeO_2 NW@SiO_2 (90 °C) < 2%Pt-CeO_2 NW@SiO_2 (70 °C). The BET surface areas of all the catalysts are shown in Table S1, However, the slight difference in surface areas seems not responsible for the differences in catalytic performances. Besides specific surface areas, other factors, *e.g.*, metal nanoparticle dispersity, material structure and the interaction between ceria and Pt probably play important effects on their catalytic performances. The high catalytic activity in Pt-CeO_2 NW@SiO_2 may be owing to the existence of more Pt-CeO_2 interfaces, which can maximums the active sites between Pt and CeO_2 [17,48]. The formation of ultra-thin Pt-CeO_2 nanowires can also benefit the dispersion of the Pt species. Though the content of Pt in 1%Pt-CeO_2 NW@SiO_2 is half of that in 2%Pt/SiO_2 and 2%Pt-CeO_2/SiO_2, its catalytic performance is better than the latter two samples.

To further investigate the reaction behavior over Pt-CeO_2 NW@SiO_2 and related catalysts, the apparent activation energy (Ea) was calculated. To exclude the mass and heat transfer limitation, the Ea values over various samples were calculated at CO conversion under 20%. The Arrhenius plots and Ea values for each sample were presented in Fig. 6(b) and Table S3. For 2%Pt-CeO_2NW@SiO_2 catalyst, its Ea value is relatively lower than the other four catalysts, which are consistent with their catalytic activity differences. As displayed in Table S3, the reaction rate on 2%Pt-CeO_2NW@SiO_2, the most active catalyst in this work, is 6.7×10^{-2} mmol g^{-1} s^{-1}, which is the maximum reaction rate

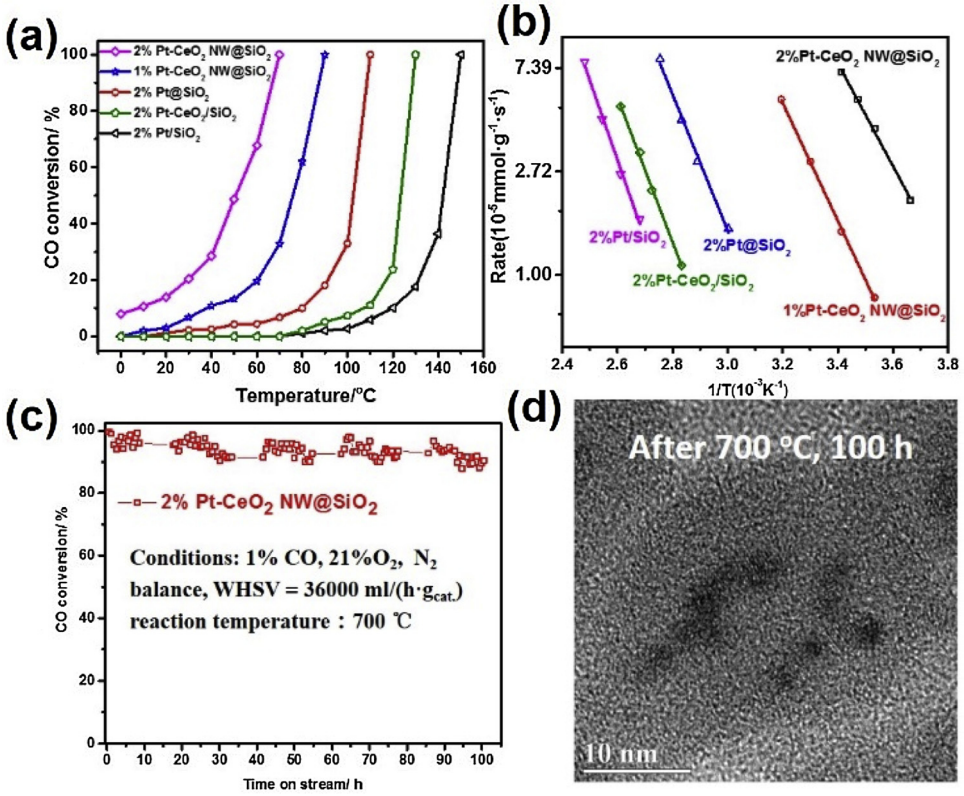

Fig. 6. (a) CO oxidation performance, (b) Arrhenius plots and (c) High temperature stability of Pt-CeO_2 NW@SiO_2; (d) TEM images of spent Pt-CeO_2 NW@SiO_2 after high temperature thermal stability test.

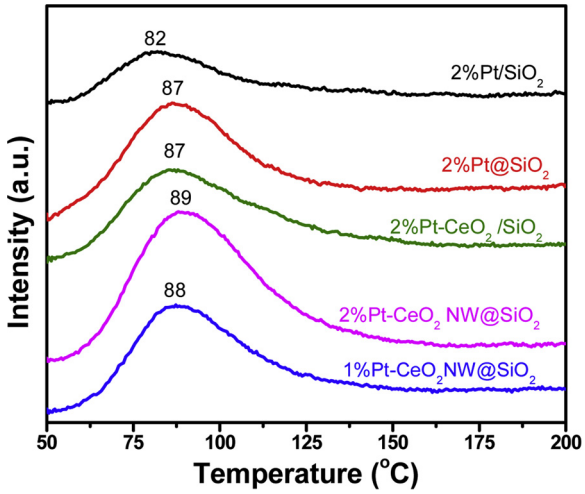

Fig. 7. CO-TPD profiles of Pt-CeO_2NW@SiO_2 and related catalysts.

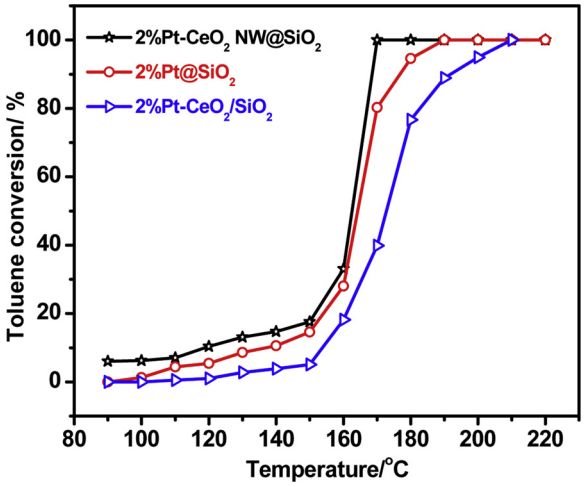

Fig. 8. Catalytic combustion of toluene over 2%Pt-CeO_2 NW@SiO_2 and related catalysts. Reaction conditions:0.030 g catalyst, 1000 ppm toluene, 40% O_2, balance N_2, total flow rate = 10 ml min^{-1}, GHSV = 20,000 ml g^{-1} h^{-1}.

among the samples.

Long-term thermal stability tests of 2%Pt-CeO_2 NW@SiO_2 at 700 °C for 100 h were also conducted. As shown in Fig. 6**(c)**, the catalyst activity barely declined. Slight aggregation is observed in TEM images of spent catalyst (Fig. 6(d)), and the spent catalyst still maintains core-shell structure with nanowires in the core. Those results indicate that the SiO_2 shell confinement can improve the thermal stability of Pt-CeO_2 NWs, and also decrease metal sintering under the conditions of high-temperature reactions. [49]

Generally speaking, over Pt based catalysts, CO molecules adsorb strongly on the outer surface of Pt NPs at low temperature, whose reaction rate is determined by the desorption of CO. The CO-TPD profiles in Fig. 7 and Table S3 demonstrate that the higher catalytic activity of the Pt-CeO_2NW@SiO_2 catalyst leads to their higher CO-desorption capability compared with other control samples. The turnover frequencies (TOF) of the exposed surface Pt active sites determined by CO-TPD method were calculated at 20 °C and the results were presented in Table S3. It can be clearly observed that 2%Pt-CeO_2 NW@SiO_2 has the highest TOF values due to the addition of CeO_2, which are six times higher than that of 2%Pt@SiO_2, and also much higher than that of 2% Pt-CeO_2/SiO_2.

The constructed Pt-CeO_2 NW@SiO_2 may act as a general catalyst, due to the high dispersion of Pt NPs, the strong Pt and CeO_2 interaction with plenty of Pt-CeO_2 interfaces, and the protection of the silica shell for Pt-CeO_2 nanowires working in high-temperature catalytic reactions. Therefore, these results encourage us to try the self-assembled Pt-CeO_2NW@SiO_2 catalyst in other catalytic reactions.

The catalytic combustion of toluene was then investigated for 2%Pt-CeO_2 NW@SiO_2, 2%Pt-CeO_2/SiO_2 and 2%Pt@SiO_2 catalysts at a temperature range of 90–220 °C in 1000 ppm of toluene, 40% O_2, and N_2 with a WHSV of 20,000 ml g^{-1} h^{-1}. Fig. 8 shows the catalytic activities of those three catalysts. The toluene conversion increased with the increasing of reaction temperature. For the 2%Pt-CeO_2 NW@SiO_2, 2%Pt-CeO_2/SiO_2 and 2%Pt@SiO_2 samples, the temperatures at toluene conversion of 90% are 167, 177, and 193 °C, respectively. Therefore, it can be obtained that the activities of the three catalysts followed the sequence of 2%Pt-CeO_2/SiO_2 < 2%Pt@SiO_2 < 2%Pt-CeO_2 NW@SiO_2. It is further verified that the incorporation of the CeO_2 can enhance the performances of the catalyst, a synergistic effect between Pt and CeO_2 and forming Pt-CeO_2 nanowires can provide more active sites in Pt-CeO_2 interface.

To further investigate the relationship between the special structure and the catalytic performance of these catalysts, the 1%Pt-CeO_2NW@SiO_2 catalyst was treated by concentrated nitric acid. In this trial, the motivation is to remove the CeO_2 nanowire in the core-shell structure. The TEM and HRTEM images of 1%Pt-CeO_2 NW@SiO_2 after treated with concentrated nitric acid are shown in Fig. 9(a–d). Pt-CeO_2 nanowires in 1%Pt-CeO_2NW@SiO_2-HNO_3 catalyst obviously disappeared compared with its pristine sample (Fig. S3), while Pt nanoparticles were retained. There is trace amount of Ce in the treated catalyst, which is confirmed by ICP-OES method. The result of Ce content can further demonstrate that CeO_2 nanowires in 1%Pt-CeO_2 NW@SiO_2 were dissolved by the concentrated nitric acid. CO oxidation activity on the 1% Pt-CeO_2 NW@SiO_2 catalysts before and after treated with concentrated nitric acid are shown in Fig. 10. 1%Pt-CeO_2 NW@SiO_2 catalyst can achieve 100% CO conversion at 90°C, however, the 1%Pt-CeO_2 NW@SiO_2-HNO_3 catalyst exhibits evidently worse activity than the original catalyst with 100% CO conversion moving higher by 30 °C due to the loss of CeO_2 nanowires, which offers Pt-CeO_2 interface and active sites to reactants, which signifies the importance of the stronger synergistic effect between Pt and CeO_2.

3.5. *In situ* DRIFTS analysis

in situ DRIFTS spectroscopy was adopted to study the CO adsorption and oxidation behavior over Pt@SiO_2, Pt-CeO_2NW@SiO_2 and Pt-CeO_2/SiO_2. Fig. 11 (A), (C) and (E) show the *in situ* DRIFT spectra of CO adsorption at 110 °C (Pt@SiO_2), 70 °C (Pt-CeO_2NW@SiO_2) and 130 °C (Pt-CeO_2/SiO_2), respectively. CO adsorbed onto these samples formed the CO vibration band at 2082 cm^{-1}, which is assigned to linearly bonded CO species on Pt active sites. [50,51] The intensity of CO adsorption decreased gradually in the sequence of Pt@SiO_2 > Pt-CeO_2 NW@SiO_2 > Pt-CeO_2/SiO_2, demonstrating that the amount of active Pt sites for CO adsorption was reduced with the increase of the Pt particle size over the Pt-CeO_2/SiO_2. CO molecules adsorb strongly with the surface active oxygen and forms various carbonate species between 1000 and 1800 cm^{-1} [52]. The same carbonate species are observed over the surface of the three catalysts, while the corresponding peaks are stronger for the Pt-CeO_2NW@SiO_2 and Pt-CeO_2/SiO_2 samples. It indicates that the Pt-CeO_2NW@SiO_2 and Pt-CeO_2/SiO_2 samples possesses more active adsorption sites. In addition, the bands at 2342 and 2360 cm^{-1} were also distinguished. The band at 2360 and 2342 cm^{-1} have been attributed to the asymmetric stretch of physiosorbed CO_2, and the intensity of CO_2 decreased gradually with the consumption of surface oxygen species. When O_2 was introduced into the steam, the intensity of the Pt−CO bands at 2082 cm^{-1} decreased notably with time for these three catalysts.

To identify adsorbed species on the three catalysts during CO oxidation reaction, the *in situ* DRIFTS analyses were further carried out to

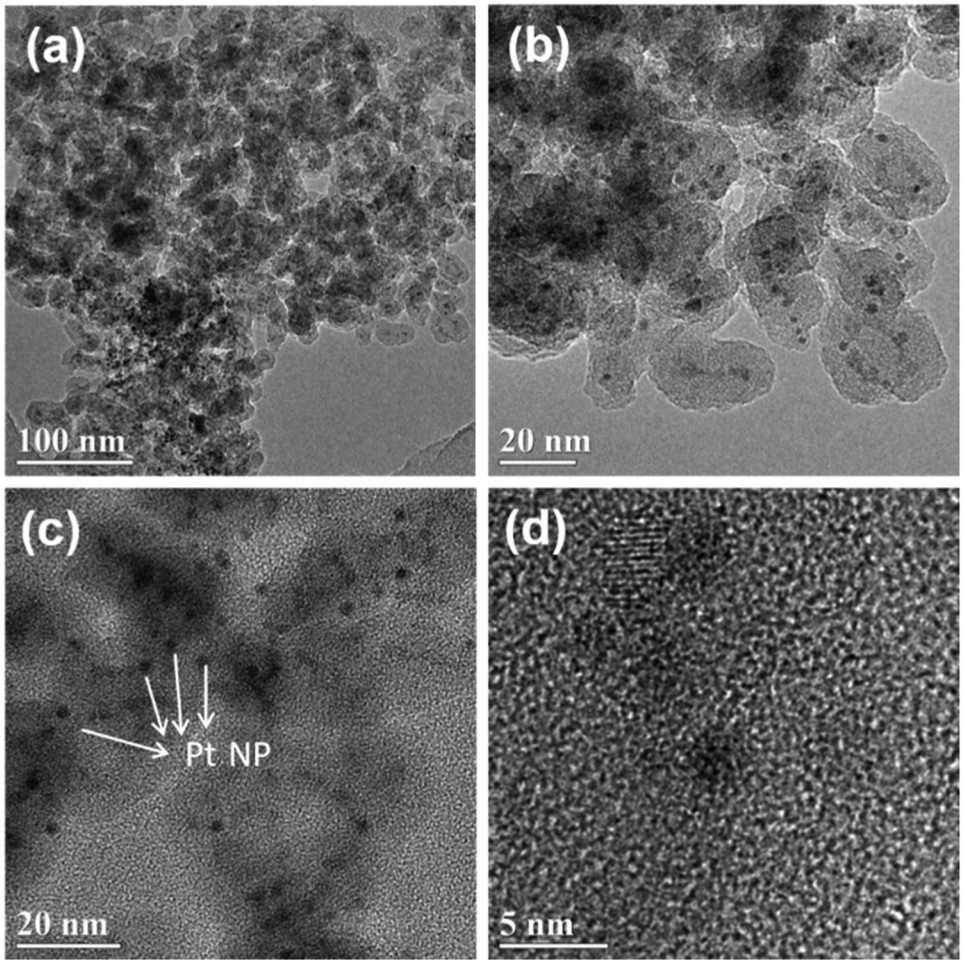

Fig. 9. TEM images of Pt-CeO_2 NW@SiO_2 treated by concentrated HNO_3 (To remove CeO_2 nanowires).

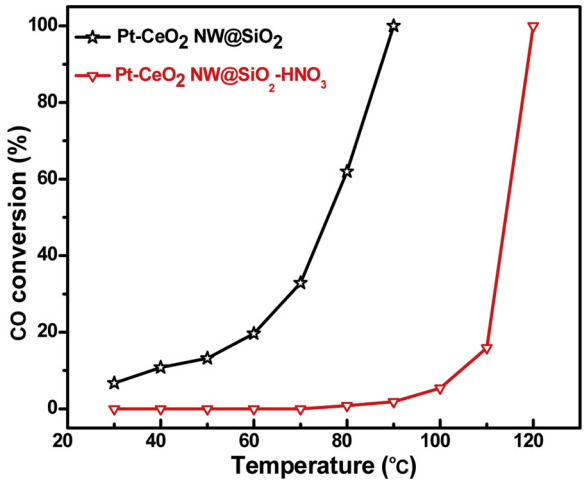

Fig. 10. Performance of 1%Pt-CeO_2 NW@SiO_2 before and treated by HNO3 for CO oxidation. Conditions: 1% CO, 21%O_2, N_2 balance, WHSV = 36,000 ml $g_{cat.}^{-1} h^{-1}$.

study CO oxidation over the three catalysts. Fig. 11 (B), (D) and (F) show DRIFT spectra of adsorbed species over the three catalysts exposed to the gas of 1 vol% CO/21 vol% O_2/78 vol% Ar at 110 °C, 70 °C and 130 °C as a function of time, respectively. When reaction gas was introduced into the steam, it was clear seen that the linear adsorption of CO on Pt sites soon over Pt-CeO_2 NW@SiO_2 and Pt@SiO_2, importantly, CO adsorption intensity over Pt-CeO_2/SiO_2 was relatively low, compared to that of Pt-CeO_2NW@SiO_2 and Pt@SiO_2. The band at 2360 and 2342 cm^{-1} have been attributed to the asymmetric stretch of physiosorbed CO_2, and the formation of CO_2 appeared gradually. It is noticed that the intensity of the bands increases in proportion to the time. The in situ DRIFT analysis confirmed that the mediate adsorption intensity of CO over Pt-CeO_2NW@SiO_2 was very important to improve its catalytic performances.

4. Conclusions

In summary, a thermally stable catalyst with a novel self-assembled Pt-CeO_2 nanowires as the core and porous silica as the shell (Pt-CeO_2NW@SiO_2) has been successfully fabricated via an *in situ* strategy. Especially, one of thinnest CeO_2 nanowire (~2 nm) was obtained via the reverse microemulsion method. The final Pt-CeO_2NW@SiO_2 displays not only an enhanced catalytic activity but also a good thermal stability for CO oxidation and toluene combustion. Compared with Pt@SiO_2 and Pt-CeO_2/SiO_2, the thermally stable Pt-CeO_2NW@SiO_2 with special core-shell nanostructure exhibits the characteristics of the high dispersion of Pt nanoparticles, low aggregate of particles, even reacted at 700 °C for 100 h. The stronger synergistic effect between Pt and CeO_2 and plenty of Pt-CeO_2 interfaces attribute to its high catalytic activity in CO oxidation and toluene combustion. The porous SiO_2 shell could offer a physical and energy barrier to prevent the migration and growth of Pt nanoparticles, which contribute to the excellent sinter-resistant ability of the catalyst. This approach is simple and efficient, which can be potentially extended to design other high performances core-shell catalysts applying in harsh reactions.

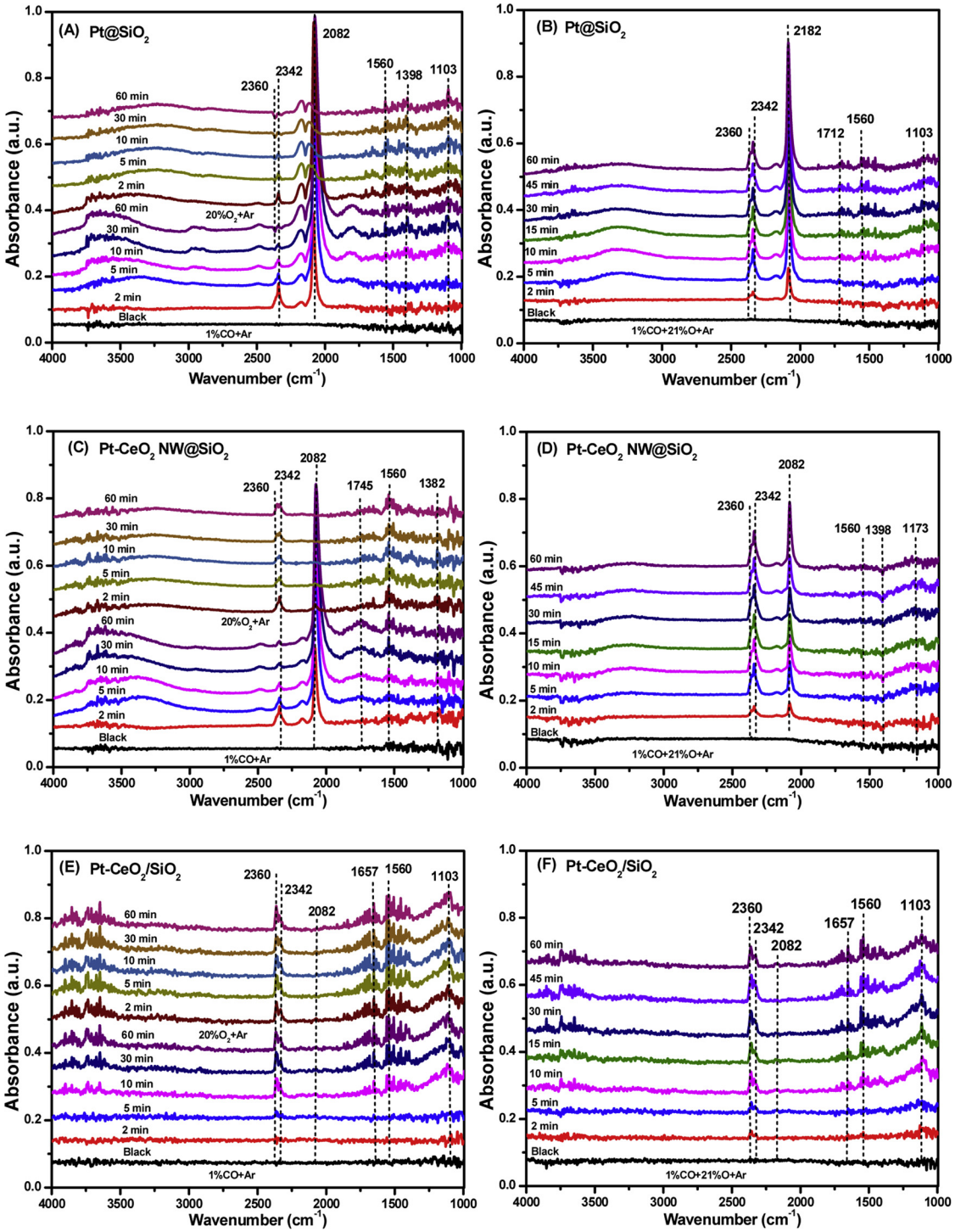

Fig. 11. Evolution of different IR bands in the 1000-2500 cm^{-1} interval for (A) $Pt@SiO_2$, (C) $Pt\text{-}CeO_2$ NW@SiO_2, and (E) $Pt\text{-}CeO_2$ /SiO_2 catalysts at 110 °C, 70 °C and 130 °C, respectively, exposed to 1 vol% CO in Ar while switching the 1 vol% CO to 20 vol% O_2 in Ar at time = 60 min. And evolution of different IR bands in the 1000-2500 cm^{-1} interval for (B) $Pt@SiO_2$, (D) $Pt\text{-}CeO_2$ NW@SiO_2, and (F) $Pt\text{-}CeO_2$ /SiO_2 catalysts at 110 °C, 70 °C and 130 °C, respectively, exposed to 1 vol % CO-21 vol % O_2-78 vol % Ar.

Acknowledgements

This work was supported by the National Key R&D Program of China (2016YFC0205900), the National Natural Science Foundation of China (21503106, 21566022 and 21773106), and the Natural Science Foundation of Jiangxi Province (20171BCB23016, 20171BAB203024 and 20181BCD4004), and the Foundation of State Key Laboratory of High-efficiency Utilization of Coal and Green Chemical Engineering (Grant No. 2018-K04). P. F. Z. acknowledges Shanghai Pujiang Program (Grant No.17PJ1403500), Thousand Talent Program, National Natural Science Foundation of China (Grant No. 21776174), and the Open Foundation of the State Key Laboratory of Ocean Engineering (Shanghai Jiao Tong University of China) (No. 1809) for the support. S. D. was supported by the Division of Chemical Sciences, Geosciences, and Biosciences, Office of Basic Energy Sciences, US Department of Energy.

Appendix A. Supplementary data

Supplementary material related to this article can be found, in the online version, at doi:https://doi.org/10.1016/j.apcatb.2019.117807.

References

[1] D. Chan, S. Tischer, J. Heck, C. Diehm, O. Deutschmann, Correlation between catalytic activity and catalytic surface area of a Pt/Al_2O_3 DOC: an experimental and microkinetic modeling study, Appl. Catal. B-Environ. 156-157 (2014) 153–165.

[2] R. Caporali, S. Chansai, R. Burch, J.J. Delgado, A. Goguet, C. Hardacre, L. Mantarosie, D. Thompsett, Critical role of water in the direct oxidation of CO and hydrocarbons in diesel exhaust after treatment catalysis, Appl. Catal. B-Environ. 147 (2014) 764–769.

[3] J. Zhao, Y. Shu, P.F. Zhang, Solid-state CTAB-Assisted synthesis of mesoporous Fe_3O_4 and $Au@Fe_3O_4$ by mechanochemistry, Chinese J. Catal. 40 (2019) 1078–1084.

[4] C. He, J. Cheng, X. Zhang, M. Douthwaite, S. Pattisson, Z. Hao, Recent advances in the catalytic oxidation of volatile organic compounds: a review based on pollutant sorts and sources, Chem. Rev. 119 (2019) 4471–4568.

[5] Y. Jian, T. Yu, Z. Jiang, Y. Yu, M. Douthwaite, J. Liu, R. Albilali, C. He, In-depth understanding of the morphology effect of α-Fe_2O_3 on catalytic ethane destruction, ACS Appl. Mater. Interfaces 11 (2019) 11369–11383.

[6] C. He, Z. Jiang, M. Ma, X. Zhang, M. Douthwaite, J.-W. Shi, Z. Hao, Understanding the promotional effect of Mn_2O_3 on Micro-/Mesoporous hybrid silica nanocubic-supported Pt catalysts for the low-temperature destruction of methyl ethyl ketone: an experimental and theoretical study, ACS Catal. 8 (2018) 4213–4229.

[7] J. Zhang, C. Rao, H. Peng, C. Peng, L. Zhang, X. Xu, W. Liu, Z. Wang, N. Zhang, X. Wang, Enhanced toluene combustion performance over Pt loaded hierarchical porous MOR zeolite, Chem.Eng. J. 334 (2018) 10–18.

[8] W. Liu, L. Zhang, T. Dong, H. Peng, Z. Wang, N. Zhang, X. Wang, P. Wu, Design of stable ultrasmall Pt−Ni(O) nanoparticles with enhanced catalytic performance: insights into the effects of Pt−Ni−NiO dual interfaces, ChemCatChem 10 (2018) 4134–4142.

[9] H. Peng, J. Ying, J. Zhang, X. Zhang, C. Peng, C. Rao, W. Liu, N. Zhang, X. Wang, La-doped Pt/TiO_2 as an efficient catalyst for room temperature oxidation of low concentration HCHO, Chinese J. Catal. 38 (2017) 39–47.

[10] D.M. Meira, R.U. Ribeiro, O. Mathon, S. Pascarelli, J.M.C. Bueno, D. Zanchet, Complex interplay of structural and surface properties of ceria on platinum supported catalyst under water gas shift reaction, Appl. Catal. B-Environ. 197 (2016) 73–85.

[11] P. Lu, B. Qiao, N. Lu, D.C. Hyun, J. Wang, M.J. Kim, J. Liu, Y. Xia, Photochemical deposition of highly dispersed Pt nanoparticles on porous CeO_2Nanofibers for the water-gas shift reaction, Adv. Funct. Mater. 25 (2015) 4153–4162.

[12] T. Yu, J. Zeng, B. Lim, Y. Xia, Aqueous-phase synthesis of Pt/CeO(2) hybrid nanostructures and their catalytic properties, Adv. Mater. 22 (2010) 5188–5192.

[13] J. Jones, H. Xiong, A.T. DeLaRiva, E.J. Peterson, H. Pham, S.R. Challa, G. Qi, S. Oh, M.H. Wiebenga, X.I. Pereira Hernández, Y. Wang, A.K. Datye, Thermally stable single-atom platinum-on-ceria catalysts via atom trapping, Science 353 (2016) 150–154.

[14] D.J. S, B. Ting, Y. Junjie, J. Yingying, W. Xiaowei, Y. Yucong, J. Yi, J. Chuanhong, Z. Hui, Y. Deren, Embedding ultrafine and high-content Pt nanoparticles at Ceria surface for enhanced thermal stability, Adv. Sci. 4 (2017) 1700056.

[15] L. Nie, D. Mei, H. Xiong, B. Peng, Z. Ren, X.I.P. Hernandez, A. DeLaRiva, M. Wang, M.H. Engelhard, L. Kovarik, A.K. Datye, Y. Wang, Activation of surface lattice oxygen in single-atom Pt/CeO2 for low-temperature CO oxidation, Science 358 (2017) 1419.

[16] C. Xie, C. Chen, Y. Yu, J. Su, Y. Li, G.A. Somorjai, P. Yang, Tandem catalysis for CO2 hydrogenation to C2–C4 hydrocarbons, Nano Lett. 17 (2017) 3798–3802.

[17] J. Su, C. Xie, C. Chen, Y. Yu, G. Kennedy, G.A. Somorjai, P. Yang, Insights into the mechanism of tandem alkene hydroformylation over a nanostructured catalyst with multiple interfaces, J. Am. Chem. Soc. 138 (2016) 11568–11574.

[18] Y. Long, S. Song, J. Li, L. Wu, Q. Wang, Y. Liu, R. Jin, H. Zhang, Pt/CeO_2@MOF Core@Shell nanoreactor for selective hydrogenation of furfural via the channel screening effect, ACS Catal. 8 (2018) 8506–8512.

[19] T. Montini, M. Melchionna, M. Monai, P. Fornasiero, Fundamentals and catalytic applications of CeO_2-Based materials, Chem. Rev. 116 (2016) 5987–6041.

[20] J.A. Rodriguez, D.C. Grinter, Z. Liu, R.M. Palomino, S.D. Senanayake, Ceria-based model catalysts: fundamental studies on the importance of the metal-ceria interface in CO oxidation, the water-gas shift, CO_2 hydrogenation, and methane and alcohol reforming, Chem. Soc. Rev. 46 (2017) 1824–1841.

[21] K. Wu, L.-D. Sun, C.-H. Yan, Recent progress in well-controlled synthesis of ceria-based nanocatalysts towards enhanced catalytic performance, Adv. Energy Mater. 6 (2016) 1600501.

[22] A. Chen, P. Holt-Hindle, Platinum-based nanostructured materials: synthesis, properties, and applications, Chem. Rev. 110 (2010) 3767–3804.

[23] S. Lee, J. Seo, W. Jung, Sintering-resistant $Pt@CeO_2$ nanoparticles for high-temperature oxidation catalysis, Nanoscale 8 (2016) 10219–10228.

[24] C. Wan, D.G. Cheng, F. Chen, X. Zhan, Fabrication of CeO_2 nanotube supported Pt catalyst encapsulated with silica for high and stable performance, Chem. Commun. (Camb.) 51 (2015) 9785–9788.

[25] J.A. Farmer, C.T. Campbell, Ceria maintains smaller metal catalyst particles by strong metal-support bonding, Science 329 (2010) 933–936.

[26] G. Zhou, P. Li, Q. Ma, Z. Tian, Y. Liu, Density functional theory plus Hubbard U study of the segregation of Pt to the CeO_{2-x} grain boundary, Nano Lett. 18 (2018) 1668–1677.

[27] Z.-c. Zhang, B. Xu, X. Wang, Engineering nanointerfaces for nanocatalysis, Chem. Soc. Rev. 43 (2014) 7870–7886.

[28] S. Chauhan, T. Mori, T. Masuda, S. Ueda, G.J. Richards, J.P. Hill, K. Ariga, N. Isaka, G. Auchterlonie, J. Drennan, Design of low Pt concentration electrocatalyst surfaces with high oxygen reduction reaction activity promoted by formation of a heterogeneous interface between Pt and CeO(x) nanowire, ACS Appl. Mater. Interfaces 8 (2016) 9059–9070.

[29] H. Zhu, Z. Wu, D. Su, G.M. Veith, H. Lu, P. Zhang, S.-H. Chai, S. Dai, Constructing hierarchical interfaces: TiO_2-Supported PtFe–FeOx nanowires for room temperature CO oxidation, J. Am. Chem. Soc. 137 (2015) 10156–10159.

[30] Q. Fu, W.-X. Li, Y. Yao, H. Liu, H.-Y. Su, D. Ma, X.-K. Gu, L. Chen, Z. Wang, H. Zhang, B. Wang, X. Bao, Interface-confined ferrous centers for catalytic oxidation, Science 328 (2010) 1141–1144.

[31] F. Dvořák, M. Farnesi Camellone, A. Tovt, N.-D. Tran, F.R. Negreiros, M. Vorokhta, T. Skála, I. Matolínová, J. Mysliveček, V. Matolín, S. Fabris, Creating single-atom Pt-ceria catalysts by surface step decoration, Nat. Commun. 7 (2016) 10801.

[32] M. Cargnello, V. Doan-Nguyen, T.R. Gordon, R.E. Diaz, E.A. Stach, R.J. Gorte, P. Fornasiero, C.B. Murray, Control of metal nanocrystal size reveals metal-support interface role for Ceria catalysts, Science 341 (2013) 771–773.

[33] S. Chauhan, G.J. Richards, T. Mori, P. Yan, J.P. Hill, K. Ariga, J. Zou, J. Drennan, Fabrication of a nano-structured Pt-loaded cerium oxide nanowire and its anode performance in the methanol electro-oxidation reaction, J. Mater. Chem. A Mater. Energy Sustain. 1 (2013) 6262.

[34] K. An, S. Alayoglu, N. Musselwhite, S. Plamthottam, G. Melaet, A.E. Lindeman, G.A. Somorjai, Enhanced CO oxidation rates at the interface of mesoporous oxides and Pt nanoparticles, J. Am. Chem. Soc. 135 (2013) 16689–16696.

[35] F. Wang, W. Li, X. Feng, D. Liu, Y. Zhang, Decoration of Pt on Cu/Co double-doped CeO2nanospheres and their greatly enhanced catalytic activity, Chem. Sci. 7 (2016) 1867–1873.

[36] F. Morfin, T.-S. Nguyen, J.-L. Rousset, L. Piccolo, Synergy between hydrogen and ceria in Pt-catalyzed CO oxidation: an investigation on $Pt–CeO_2$ catalysts synthesized by solution combustion, Appl. Catal. B-Environ. 197 (2016) 2–13.

[37] S. Ramani, S. Sarkar, V. Vemuri, S.C. Peter, Chemically designed CeO_2 nanoboxes boost the catalytic activity of Pt nanoparticles toward electro-oxidation of formic acid, J. Mater. Chem. A Mater. Energy Sustain. 5 (2017) 11572–11576.

[38] S. Bai, L. Bu, Q. Shao, X. Zhu, X. Huang, Multicomponent Pt-Based zigzag nanowires as selectivity controllers for selective hydrogenation reactions, J. Am. Chem. Soc. 140 (2018) 8384–8387.

[39] N. Zhang, L. Bu, S. Guo, J. Guo, X. Huang, Screw thread-like platinum–Copper nanowires bounded with high-index facets for efficient electrocatalysis, Nano Lett. 16 (2016) 5037–5043.

[40] M. Li, Z. Zhao, T. Cheng, A. Fortunelli, C.-Y. Chen, R. Yu, Q. Zhang, L. Gu, B. Merinov, Z. Lin, E. Zhu, T. Yu, Q. Jia, J. Guo, L. Zhang, W.A. Goddard, Y. Huang, X. Duan, Ultrafine jagged platinum nanowires enable ultrahigh mass activity for the oxygen reduction reaction, Science 354 (2016) 1414–1419.

[41] E.W. Zhao, R. Maligal-Ganesh, C. Xiao, T.W. Goh, Z. Qi, Y. Pei, H.E. Hagelin-Weaver, W. Huang, C.R. Bowers, Silica-encapsulated Pt-Sn intermetallic nanoparticles: a robust catalytic platform for parahydrogen-induced polarization of gases and liquids, Angew. Chem. Int. Ed. 56 (2017) 3925–3929.

[42] H. Peng, C. Rao, N. Zhang, X. Wang, W. Liu, W. Mao, L. Han, P. Zhang, S. Dai, Confined ultrathin Pd-Ce nanowires with outstanding moisture and SO_2 tolerance in methane combustion, Angew. Chem. Int. Ed. 57 (2018) 8953–8957.

[43] C. Rao, C. Peng, H. Peng, L. Zhang, W. Liu, X. Wang, N. Zhang, P. Wu, In situ embedded Pseudo pd–Sn solid solution in Micropores Silica with remarkable catalytic performance for CO and propane oxidation, ACS Appl. Mater. Interfaces 10 (2018) 9220–9224.

[44] Z.A. Qiao, P. Zhang, S.H. Chai, M. Chi, G.M. Veith, N.C. Gallego, M. Kidder, S. Dai, Lab-in-a-shell: encapsulating metal clusters for size sieving catalysis, J. Am. Chem. Soc. 136 (2014) 11260–11263.

[45] W. Liu, L. Li, X. Zhang, Z. Wang, X. Wang, H. Peng, Design of $Ni-ZrO_2@SiO_2$catalyst with ultra-high sintering and coking resistance for dry reforming of methane to prepare syngas, J. CO_2 Util. 27 (2018) 297–307.

[46] Z. Li, Z. Wang, B. Jiang, S. Kawi, Sintering resistant Ni nanoparticles exclusively confined within SiO_2 nanotubes for CH_4 dry reforming, Catal. Sci. Technol. 8 (2018) 3363–3371.

[47] H. Peng, X. Zhang, L. Zhang, C. Rao, J. Lian, W. Liu, J. Ying, G. Zhang, Z. Wang, N. Zhang, X. Wang, One-pot facile fabrication of multiple nickel nanoparticles confined in microporous silica giving a Multiple-Cores@Shell structure as a highly efficient catalyst for methane dry reforming, ChemCatChem 9 (2017) 127–136.

[48] H.-P. Zhou, H.-S. Wu, J. Shen, A.-X. Yin, L.-D. Sun, C.-H. Yan, Thermally stable $Pt-CeO_2$ hetero-nanocomposites with high catalytic activity, J. Am. Chem. Soc. 132 (2010) 4998–4999.

[49] S.H. Joo, J.Y. Park, C.-K. Tsung, Y. Yamada, P. Yang, G.A. Somorjai, Thermally stable Pt/mesoporous silica core–shell nanocatalysts for high-temperature reactions, Nat. Mater. 8 (2008) 126.

[50] S.M. McClure, D.W. Goodman, Simulating the complexities of heterogeneous catalysis with model systems: case studies of SiO_2 supported Pt-Group metals, Top. Catal. 54 (2011) 349–362.

[51] X. Wang, D. Liu, S. Song, H. Zhang, $Pt@CeO_2$ multicore@shell self-assembled nanospheres: clean synthesis, structure optimization, and catalytic applications, J. Am. Chem. Soc. 135 (2013) 15864–15872.

[52] Y. Zheng, K. Li, H. Wang, Y. Wang, D. Tian, Y. Wei, X. Zhu, C. Zeng, Y. Luo, Structure dependence and reaction mechanism of CO oxidation: a model study on macroporous CeO_2 and CeO_2-ZrO_2 catalysts, J. Catal. 344 (2016) 365–377.